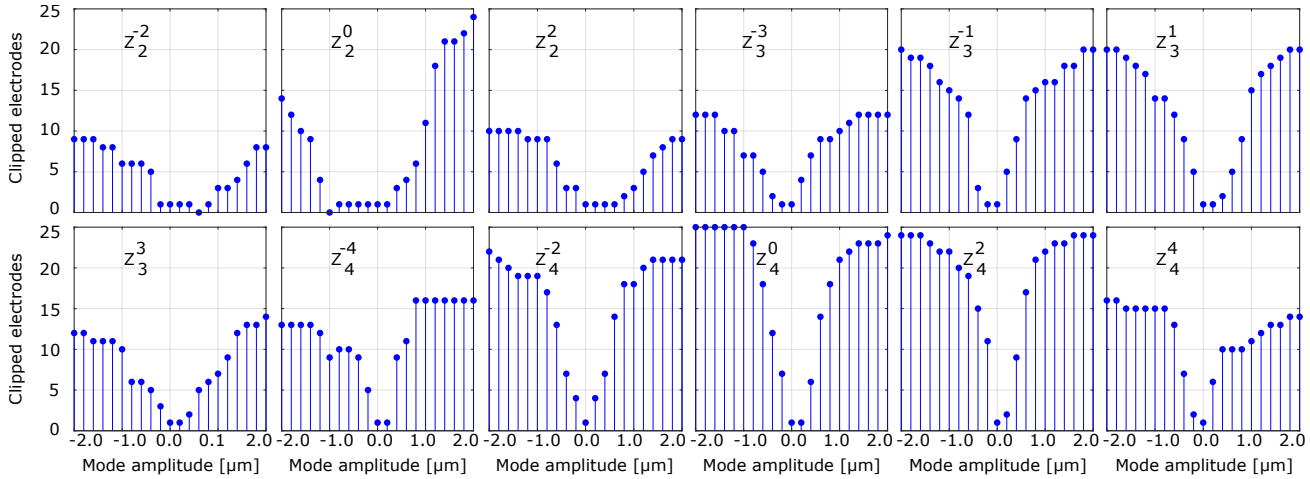

Figure 8. Clipping condition of the deformable mirror's electrodes while reproducing Zernike modes for an amplitude sweep between $-2\,\mu m$ to $2\,\mu m$ with steps of $0.2\,\mu m$ and controlled by SVD. In the SVD method, when the obtained control signals exceed the system boundaries they are clipped at the maximum/minimum possible values.

6. CONCLUSION

We presented a novel optimization-based open-loop control strategy to replace the conventional pseudo-inversion-based control techniques for driving the phase modulators within adaptive optics systems. A convex non-equality constrained least squares optimization problem was formulated and an interior-point method was used to solve the problem. The proposed control system was implemented on two electrostatically-actuated phase modulators; a deformable mirror and an optofluidic refractive phase modulator. It was experimentally shown that both of the phase modulators perform significantly better when controlled by the optimization-based control compared to when they are controlled by the conventional SVD-based method. We demonstrated that when a large number of actuation signals exceed the boundary limits of the system, the optimization-based control can find the global optimal control signals inside the feasible voltage range to conserve the fidelity of the replicated Zernike modes.

APPENDIX A. QUANTITATIVE PHASE MEASUREMENT

Spatial-carrier fringe-pattern analysis technique is used for extracting the phase data from the captured interferograms.[14] Compared to other methods for quantitative phase measurement, this technique has the advantage of capturing all the phase data in a single frame and therefore is a suitable option for real-time interferometry. For the reflective phase modulator a Micheloson-type interferometer and for the refractive phase modulator a Mach-Zehnder-type interferometer is used to generate the interferograms.

Figure 9 summarizes the different steps of this technique. An example of an captured interferogram is shown in figure 9a while the fringe pattern shown in figure 9b depicts its subset of area of interest. The fringe pattern is composed of 3 sets of data:

- Desired phase modulation that is induced by the phase modulator, placed in the measurement arm of the interferometer
- Irradiance variations due to the non-uniform light reflection or transmission by the phase modulator
- Noise

The first two of the above-mentioned data have low spatial frequency and therefore, by taking Fourier Transform (FT) of the interferogram, their spatial frequencies are all concentrated in a low frequency spectra in the center of the frequency domain. This is visible in figure 9c which shows the spectral density of the interferogram (absolute of its FT). In order to be able to separate the desired phase modulation from the unwanted irradiance, a common practice is to introduce a pattern with relatively large spatial-frequency. This

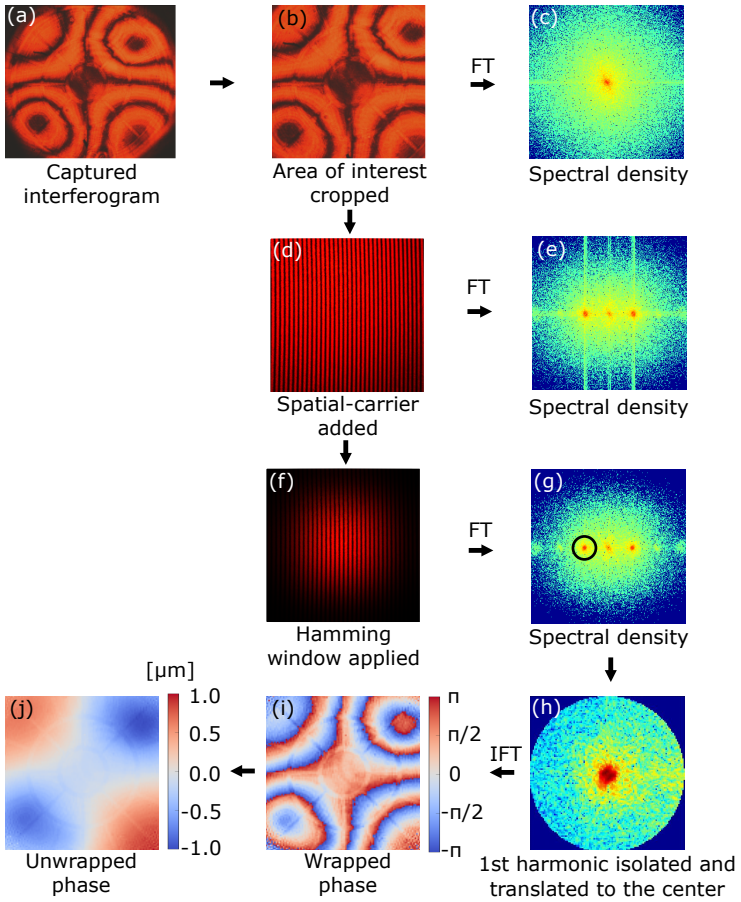

Figure 9. Summary of the spatial-carrier fringe-pattern analysis technique for extracting quantitative phase data from the captured interferograms.

is called the spatial-carrier which is in form of sinusoidal fringes with repetition frequency of f_0 and is added to the system by tilting one of the interferometer's mirrors. Figure 9d shows the interferogram after adding the spatial-carrier. By doing this, the desired phase modulations are carried by the added sinusoidal pattern and in the frequency domain they are shifted by the sinus-frequency f_0 from the origin, while the unwanted background irradiance data remain in the center spectra (figure 9e).

The strong vertical lines in the Fourier spectra (figure 9e), which are caused due to discontinuity of data at the edges and sharp interferogram boundaries, can be compensated by applying a 2D analog of Hamming window to the interferogram in spatial domain.[17] Figure 9f shows the interferogram of the area of interest after multiplying it by the hamming window and figure 9g shows its spectral density. Either of the two spectra on the carrier, which are visible as two harmonic lobes by their local contrast at the sides of the origin's lobe, include the desired phase data and can be expressed by $C(f_x - f_0, f_y)$ where f_x and f_y are the spatial frequency in the x and y directions respectively. By sufficient filtering of one of the two harmonic lobes (here the one shown with the black circle in figure 9g is chosen), the unwanted background irradiance variation is removed. Next by translating the filtered spectra by f_0 towards the origin, the carrier frequency is removed which results in $C(f_x, f_y)$ (figure 9h). Taking the Inverse Fourier Transform (IFT) of the isolated spectra gives[14]

$$c(x, y) = \frac{1}{2} b(x, y) \exp[i\phi(x, y)], \tag{8}$$

where x and y are the spatial coordinates, $b(x, y)$ is the amplitude variation of the isolated spectra and $\phi(x, y)$ is the desired phase modulation. Using equation 8 and simple mathematical operations it is possible to calculate

$\phi(x, y)$. The obtained phase is constrained in the range $(-\pi, \pi]$ or $[0, 2\pi)$ and thus is called the wrapped phase as depicted in figure 9i. If the frequency filter, considering its size and position, adequately separate the spectra of the desired phase modulation, the wrapped phase has to resemble the fringe pattern of the interferogram before adding the spatial-carrier. The following points are important for precise filtering of the first harmonic:

- In the Fourier domain, spectrum of first harmonic lobe should not overlap with the spectrum of the background irradiance and the higher order lobes.
- The frequency filter has to encompass the whole spectra of the 1st order lobe. Here a circular filter is utilized. However usage of other frequency shapes such as square, rectangle and even free shapes can be found in literature.[18]
- The position of the filter has a significant effect on the accuracy of the measurements. Ideally, the center of the filter should have a distance equal to the carrier frequency from the origin. However, because of the discrete nature of the data, the appropriate position of the filter center might be in between two pixels. Such situations may be alleviated by use of a high resolution sensor or can be compensated by adjusting the carrier frequency or diameter of the filter.

Wrapped phase needs to go through an unwrapping routine to give a continuous phase map. The employed unwrapping function for this work was introduced by Costantini.[19] The calculated phase modulation can be represented with the unit of length by multiplying it with the wavelength of the utilized laser for interferometry (here $\lambda = 632\,\text{nm}$). The overall obtained accuracy of this method under controlled conditions is proved to be $\lambda/100$.[17]

FUNDING INFORMATION

This work is partially supported by the Deutsche Forschung Gemeinschaft (DFG) (Project 62751: OFAO).

REFERENCES

[1] Tyson, R., [*Principles of adaptive optics*], CRC press, Boca Raton (2010).
[2] Booth, M. J., "Adaptive optical microscopy: the ongoing quest for a perfect image," *Light: Science & Applications* **3**(4), e165 (2014).
[3] Ji, N., "Adaptive optical fluorescence microscopy," *Nature Methods* **14**(4), 374 (2017).
[4] Hell, S. W., Sahl, S. J., Bates, M., Zhuang, X., Heintzmann, R., Booth, M. J., Bewersdorf, J., Shtengel, G., Hess, H., Tinnefeld, P., et al., "The 2015 super-resolution microscopy roadmap," *Journal of Physics D: Applied Physics* **48**(44), 443001 (2015).
[5] Patton, B. R., Burke, D., Owald, D., Gould, T. J., Bewersdorf, J., and Booth, M. J., "Three-dimensional STED microscopy of aberrating tissue using dual adaptive optics," *Optics Express* **24**(8), 8862–8876 (2016).
[6] Salter, P. S., Woolley, M. J., Morris, S. M., Booth, M. J., and Fells, J. A., "Femtosecond fiber bragg grating fabrication with adaptive optics aberration compensation," *Optics Letters* **43**(24), 5993–5996 (2018).
[7] Devaney, N., Dalimier, E., Farrell, T., Coburn, D., Mackey, R., Mackey, D., Laurent, F., Daly, E., and Dainty, C., "Correction of ocular and atmospheric wavefronts: a comparison of the performance of various deformable mirrors," *Applied Optics* **47**(35), 6550–6562 (2008).
[8] Devaney, N., Coburn, D., Coleman, C., Dainty, J. C., Dalimier, E., Farrell, T., Lara, D., Mackey, D., and Mackey, R., "Characterisation of mems mirrors for use in atmospheric and ocular wavefront correction," in [*MEMS Adaptive Optics II*], **6888**, 688802, International Society for Optics and Photonics (2008).
[9] Banerjee, K., Rajaeipour, P., Ataman, Ç., and Zappe, H., "A low-cost, 25-actuator electrostatic deformable mirror with polyimide membrane for adaptive optics microscopy," in [*MOEMS and Miniaturized Systems XVII*], **10545**, 105450G, International Society for Optics and Photonics (2018).
[10] Banerjee, K., Rajaeipour, P., Ataman, Ç., and Zappe, H., "Optofluidic adaptive optics," *Applied Optics* **57**(22), 6338–6344 (2018).

[11] Banerjee, K., Rajaeipour, P., Ataman, Ç., and Zappe, H., "An optofiuidic refractive phase modulator with an electrostatic 2d actuator array," in [*2018 International Conference on Optical MEMS and Nanophotonics (OMN)*], 1–2, IEEE (2018).

[12] Fischer, D. J., O'Bryan, J. T., Lopez, R., and Stahl, H. P., "Vector formulation for interferogram surface fitting," *Applied Optics* **32**(25), 4738–4743 (1993).

[13] Nocedal, J. and Wright, S. J., [*Numerical optimization 2nd edition*], Springer, New York (2006).

[14] Takeda, M., Ina, H., and Kobayashi, S., "Fourier-transform method of fringe-pattern analysis for computer-based topography and interferometry," *JosA* **72**(1), 156–160 (1982).

[15] Andersson, J. A., Gillis, J., Horn, G., Rawlings, J. B., and Diehl, M., "Casadi: a software framework for nonlinear optimization and optimal control," *Mathematical Programming Computation* , 1–36 (2018).

[16] Wächter, A. and Biegler, L. T., "On the implementation of an interior-point filter line-search algorithm for large-scale nonlinear programming," *Mathematical Programming* **106**(1), 25–57 (2006).

[17] Kujawinska, M. and Wojciak, J., "High accuracy fourier transform fringe pattern analysis," *Optics and lasers in engineering* **14**(4-5), 325–339 (1991).

[18] Breluzeau, C., Bosseboeuf, A., Petitgrand, S., and Leroux, X., "Automated fringe-pattern extrapolation for patterned surface profiling by interference microscopy with fourier transform analysis," in [*Nano-and Micro-Metrology*], **5858**, 58580B, International Society for Optics and Photonics (2005).

[19] Costantini, M., "A novel phase unwrapping method based on network programming," *IEEE Transactions on geoscience and remote sensing* **36**(3), 813–821 (1998).